Received: 28 May 2020 | Revised: 2 October 2020 | Accepted: 19 October 2020

DOI: 10.1049/rsn2.12061

IET Radar, Sonar & Navigation

The Institution of Engineering and Technology WILEY

ORIGINAL RESEARCH PAPER

Multi-carrier and multi-polarimetric model based adaptive target detector for passive radar systems

Francesca Filippini | **Fabiola Colone**

Department of Information Engineering, Electronics and Telecommunications (DIET), Sapienza University of Rome, Rome, Italy

Correspondence

Francesca Filippini, Department of Information Engineering, Electronics and Telecommunications (DIET), Sapienza University of Rome, Rome, Italy.
Email: francesca.filippini@uniroma1.it

Funding information

The work has been partially supported by MIUR (Italian Ministry of Education, University and Research) under the project "S4E – Safety & Security Systems for Sea Environment " – identification code SCN 00393

Abstract

A new adaptive detection strategy for passive radar systems that fruitfully capitalizes on signals, simultaneously emitted by the same transmitter of opportunity at different carrier frequencies and collected by a set of differently polarized surveillance antennas is derived. Based on recent results that demonstrated the benefits provided by proper strategies to exploit polarimetric diversity, the authors aim at further improving the target detection performance by combining polarimetric and frequency diversity. Real data collected through an FM radio-based passive radar prototype is used to extensively demonstrate the effectiveness of the derived strategy with respect to state-of-the-art approaches. The conceived solution is proved to successfully enhance the capability to discriminate targets, thanks to an effective disturbance rejection performed at each frequency channel as well as a target echo enhancement and an increased robustness to the time-varying characteristics of the exploited source of opportunity.

1 | INTRODUCTION

Passive bistatic radar (PBR), or passive coherent location (PCL), technology exploits signals emitted by illuminators of opportunity (IOs) to detect and localize targets [1, 2]. The advantages of such sensors, that is, the reduced costs of realization and maintenance, the low vulnerability to electronic countermeasures or the possibility to be deployed in areas where conventional active radars would not be allowed, just to mention a few, are well known and have attracted significant research interest in the past decades.

Different sources of opportunity have been considered in the literature; however, broadcast IOs, such as FM radio, digital audio or video broadcasting services (DAB or DVB-T), are usually preferred for their wide coverage [3–7]. In addition, broadcast IOs typically simultaneously transmit multiple signals at different carrier frequencies which inherently offer an information diversity that can be fruitfully exploited, as investigated in [8–12]. Frequency diversity was proved to be useful to achieve wider bandwidths, resulting in finer range resolutions, see for example [8–10] where the coherent integration of different frequency channels was used. On the other hand, in [11, 12] the combination of multiple frequency channels was shown to increase the target detection performance and the robustness of the system with respect to interference contributions, by non-coherently combining the outputs obtained at different carriers. The latter advantage was demonstrated with both FM radio and DVB-T IOs, however the analyses conducted have also demonstrated that the achievable performance might significantly vary depending on the number and the quality of the available set of frequency channels. Therefore, a proper maximization of the performance at the single frequency (SF) channel is desirable. To this purpose, several advanced processing strategies have been conceived.

One possibility is represented by the combination of signals collected using differently polarized receiving antennas [13–21]. First attempts to exploit polarimetric diversity have been pursued in [12–14], where a simple non-coherent integration (NCI) of the different polarimetric signals was proposed and shown to increase the target signal to noise ratio (SNR). A more effective polarimetric adaptive approach was derived in [16] by resorting to a locally adaptive generalized likelihood ratio test (GLRT) strategy applied over the range-Doppler plane. Recently, the authors in [18, 19] have derived an adaptive target detector by resorting to a parametric approach, namely by modelling the disturbance as a multi-channel autoregressive (AR) process. The derived detector,

referred to as modified polarimetric AR model based adaptive matched filter (Mod-Pol-AR-AMF) has been efficiently adapted to the PCL case in [20, 21] and extensively tested and validated against real data. The results in [21] have demonstrated that the detection performance achievable at the SF channel can be remarkably increased thanks to a proper exploitation of the polarimetric and temporal correlation to counteract the disturbance.

Based on the substantial improvement that the Mod-Pol-AR-AMF yields at a SF channel, in this work, we extend the conceived approach to a multi-frequency (MF) scenario. We derive a novel adaptive target detector that efficiently leverages signals collected by differently polarized antennas at different frequency channels. The joint exploitation of polarimetric and frequency diversity was considered in [22], where the polarimetric locally adaptive GLRT detection strategy was employed in conjunction with the MF approach. However, further improvements are expected if the MF integration benefits from a more effective preliminary processing stage that successfully maximizes the performance at the SF channel. To assess the benefits of the proposed detector, we carry out an extensive performance analysis against real data collected using an FM radio based PCL system. Preliminary results along this line are reported in [23]. The experimental validation demonstrates that the proposed solution effectively increases the target detection capability with respect to the strategies that separately exploit polarimetric and frequency diversity as well as with respect to the multi-carrier and multi-polarimetric state-of-the-art approach. Finally, we carry out a comparison of the computational complexity required by the considered strategies, providing useful guidelines for an appropriate selection of the information sources to be exploited.

The reminder of the paper is organized as follows. In Sections 2 and 3, we briefly describe the detection strategies that separately leverage the frequency and polarimetric diversity. Section 4 is devoted to the derivation of the proposed multi-polarimetric and multi-frequency adaptive parametric detector. In Section 5, we carry out an extensive performance assessment of the proposed solution against real data and we report a complete analysis of its computational complexity. Eventually, we report our concluding remarks in Section 6.

2 | EXPLOITATION OF FREQUENCY DIVERSITY AT THE SINGLE POLARIMETRIC CHANNEL

Let us consider a multi-channel PCL system that collects signals simultaneously transmitted by the same IO at N different carrier frequencies from L differently polarized surveillance antennas. In this section, we briefly describe an effective MF target detector applied at the lth single polarimetric (SP) channel, $l = 0, \ldots, L-1$.

The first step of a conventional PCL processing is represented by a temporal disturbance cancelation stage, separately applied at each of the NL available signals. This stage aims at reducing the direct signal, clutter and multipath contributions and it relies on the availability of a good copy of the transmitted waveform collected by a dedicated reference antenna and can be performed according to different solutions, see for example [2, 24].

Afterwards, according to the approach proposed in [11] the N surveillance signals at the lth polarimetric channel ($l = 0, \ldots, L-1$) separately undergo the cross-ambiguity function (CAF) evaluation. Once N CAFs are available, they are jointly exploited based on an appropriate combination strategy among those introduced in [11]. In this paper we use a centralized NCI strategy, followed by a cell average constant false alarm rate (CA-CFAR) detection scheme.

More precisely, for a given cell under test (CUT) at delay-Doppler location (τ, f_D), we collect the complex values extracted from the N CAFs at the lth polarimetric channel in an N–dimensional complex vector $\mathbf{y}_l^{MF}(\tau, f_D)$, $l = 0, \ldots, L-1$. By assuming that the disturbance is independent at the different frequency channels, we model $\mathbf{y}_l^{MF}(\tau, f_D)$ as a complex white Gaussian vector, and we obtain the adaptive target detector as follows [11].

$$\frac{\|\mathbf{y}_l^{MF}(\tau, f_D)\|^2}{\sum_{p \in I_{(\tau f_D)}} \|\mathbf{y}_l^{MF}(\tau_p, f_{Dp})\|^2} \gtrless T_{MF} \tag{1}$$

where the average intensity is estimated over P secondary data surrounding the CUT ($\mathbf{y}_l^{MF}(\tau_p, f_{Dp})$, $p \in I_{(\tau f_D)}$, $|I_{(\tau f_D)}| = P$).

The detection threshold T_{MF} is selected by inverting the following expression of the false alarm probability (P_{fa})

$$P_{fa} = \sum_{n=0}^{N-1} \binom{PN + n - 1}{n} \left(\frac{T}{PN}\right)^n \left(1 + \frac{T}{PN}\right)^{-PL-n} \tag{2}$$

The centralized MF-NCI approach has been extensively applied to real data, using signals transmitted by different IOs, for example FM radio [11] and DVB-T [12]. The results reported therein clearly show that it yields a significant enhancement in terms of target detection capability with respect to the SF operation. The obtained improvement is due to the expected enhancement of the target echo resulting from the NCI, but also to the capability of averaging the characteristics of the employed channels. However, the achievable performance might significantly change depending on the number and quality of the exploited frequency channels. Given these considerations, it is expected that the target detection performance obtained with the MF approach would further benefit from a proper performance maximization operated at the SF channel.

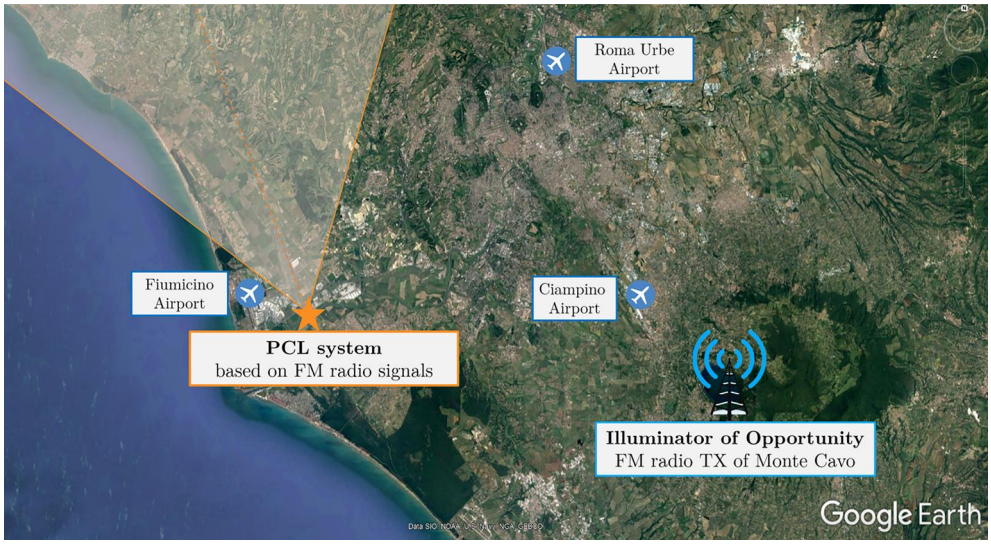

FIGURE 1 Acquisition geometry

3 | EXPLOITATION OF POLARIMETRIC DIVERSITY AT THE SINGLE FREQUENCY CHANNEL

In this section, we briefly describe two different detection strategies that exploit signals collected at the nth carrier frequency, $n = 0, \ldots, N-1$, with multi-polarized surveillance antennas.

Once the temporal disturbance cancelation stage has been performed, L sequences of M samples are available at the nth frequency channel, denoting M as the number of samples in the considered CPI. Depending on the considered polarimetric detection scheme, they will undergo different processing stages that are briefly described in the following subsections.

3.1 | Polarimetric GLRT applied over the range-Doppler plane

According to the Polarimetric GLRT detection strategy introduced in [16, 17] first L CAFs are evaluated at the nth frequency channel. The output of this stage is a set of bistatic range-velocity maps containing both targets echoes and disturbance contributions, such as thermal noise, cancelation residuals and interference. For a given CUT, the results of the L channels at the nth carrier frequency are collected in a complex L-dimensional vector $\mathbf{y}_n^{MP}(\tau, f_D)$. We assume that vector $\mathbf{y}_n^{MP}(\tau, f_D)$follows a complex Gaussian distribution with a disturbance covariance matrix $\mathbf{M}_n$ and mean vector $\mathbf{0}$ or $\mathbf{s}_n = [\alpha_{n,0} \ \ldots \ \alpha_{n,L-1}]^T$ under the H_0 (target absent) or H_1 (target present) hypothesis, respectively, where $\mathbf{s}_n$ is the vector of unknown complex amplitudes at the L polarimetric channels at the nth SF channel. Also, P secondary vectors are assumed available, $\mathbf{y}_n^{MP}(\tau_p, f_{Dp})$, $p \in I_{(\tau f_D)}$, $|I_{(\tau f_D)}| = P$, independent and identically distributed (i.i.d), with the same statistic of $\mathbf{y}_n^{MP}(\tau, f_D)$, under the null hypothesis and extracted from the set of range-Doppler indices $I_{(\tau f_D)}$adjacent to the CUT.

By resorting to the GLRT approach, the detection test derived in [16] is obtained as:

$$\mathbf{y}_n^{MPH}(\tau, f_D)\hat{\mathbf{M}}_n^{-1}(\tau, f_D)\mathbf{y}_n^{MP}(\tau, f_D) \gtrless T_{Pol-GLRT} \tag{3}$$

where $\hat{\mathbf{M}}_n(\tau, f_D) = \sum_{p=1}^{P} \mathbf{y}_n^{MP}(\tau_p, f_{Dp})\mathbf{y}_n^{MPH}(\tau_p, f_{Dp})$ is the estimated sample covariance matrix and $T_{Pol-GLRT}$ is the detection threshold, selected according to the following P_{fa} expression

$$P_{fa} = \frac{(1-\kappa)^{P-L+1}}{(P-L)!} \sum_{l=0}^{L-1} \frac{\Gamma(P-l)}{\Gamma(L-l)} \kappa^{L-l+1} \tag{4}$$

being $T = \kappa\,(1-\kappa)^{-1}$ and $\Gamma(\cdot)$ denotes the Gamma function. It is worth noticing that the Pol-GLRT can be interpreted as the cascade of a whitening transformation on the range-Doppler domain by means of the Cholesky decomposition of the estimated matrix $\hat{\mathbf{M}}_n$, followed by an NCI of the whitened output. It was proved in [16, 17] that the whitening stage prior to the integration allows to counteract the disturbance and to improve the target discrimination capability with respect to a simple NCI performed along the polarimetric domain according to the so called Pol-NCI approach [13].

The effectiveness of this strategy is shown in the following on real data, collected during an experimental campaign carried out near Fiumicino Airport, in Italy, (see Figure 1), using a FM radio-based PCL prototype [16]. Two dual-polarized log periodic antennas were used as surveillance and reference antenna, respectively. Each of them is equipped with two independent outputs, one vertical (V) and one horizontal (H) polarized ($L = 2$). The considered dataset is composed by 2060 datafiles

TABLE 1 Available FM radio channels

	Carrier Frequency (MHz)	FM Radio Broadcast	Transmitter Polarization
f_0	91.2	RAI R.2	H
f_1	92.4	RTL	V
f_2	94.5	SUBASIO	V
f_3	103.2	RDS	V

of 1.1s each, for a total acquisition of 80 min. The employed setup allows collecting data from up to four different FM radio channels ($N = 4$), each one from four different antennas. Details on the set of four FM radio channels exploited in this work are reported in Table 1. Specifically, the employed signals are simultaneously transmitted by the FM radio IO, located in Monte Cavo, approx. 35 km away from the PCL receiver (see Figure 1). The air-truth for the same air space has been provided by the SBS-1 real time virtual radar. Additional details on the acquisition campaign are reported in [16].

Figure 2 reports an example of the results obtained over a single datafile. More precisely, Figure 2a,b show the outputs of a conventional CA autogate applied over the CAFs separately obtained at the two available polarimetric surveillance channels after the temporal disturbance cancelation.

Figure 2c shows the outputs of the polarimetric whitening stage for the H channel at each range-Doppler bin in the map, before the final NCI. Similar results are obtained for the V channel. Finally, Figure 2d reports the output of the Pol-GLRT strategy. All figures have been scaled to the noise floor power level for a direct comparison.

In Figure 2a,b,d, the white circles represent the position of the available air-truth at the time of the considered datafile, while the bold green circles indicate the targets that have been correctly detected by the PCL system with a $P_{fa} = 10^{-3}$ when employing a conventional CA-CFAR detector (Figure 2a,b) or the Pol-GLRT thresholding stage in Equation (3) (Figure 2d).

Observing Figure 2a,b, (i) the effect of the temporal disturbance cancellation is evident around the zero-Doppler; (ii) the background level at the SP channels might be significantly higher than the nominal system noise level (0 dB), confirming that the surveillance signal is likely to be severely corrupted by cochannel and adjacent-channel interference, as well as disturbance cancellation residuals and thermal noise, as demonstrated in [16]; (iii) depending on the adopted polarization on receive, the detection results might be different.

By observing Figure 2c, instead, the background level is considerably reduced, thanks to an effective interference rejection obtained exploiting the polarimetric information. Finally, Figure 2d shows that a few additional detections would be obtained at this datafile if the whitened outputs also undergo the following NCI stage.

To further prove the effectiveness of this approach, we report in Figure 3 the normalized histograms of the phase differences measured at each range-velocity bin between the H and V map before and after the polarimetric whitening. The blue histogram, that shows the correlation characteristics of the CAFs separately obtained at the available channels, namely before the polarimetric information is exploited, and has a spiky behaviour denoting the presence of a common interfering source. The orange histogram, instead, measured on the H and V maps after the polarimetric whitening, shows a quite uniform trend as it would be expected in the presence of thermal noise only, revealing that the undesired interference contributions have been effectively rejected.

Figures 2 and 3 have clearly shown the effectiveness of the Pol-GLRT strategy. However, the whitening stage included therein is performed using the polarimetric information only, neglecting the temporal correlation of the disturbance. Therefore, further improvements are expected if the temporal information is also capitalized.

3.2 | Modified polarimetric AR model based adaptive matched filter

An effective solution that jointly operates in the polarimetric and the temporal domains was proposed by the authors in [18, 19] where a parametric adaptive detector was derived for a generic multi-polarimetric radar system. Then, it was efficiently adapted to the case of a PCL system in [21]. This approach is based on using a multi-channel AR process to approximate the spectral characteristics of the residual disturbance affecting the polarimetric surveillance channels after the first cancelation stage, with the aim to reduce the computational complexity of conventional fully adaptive polarimetric detection schemes.

In detail, for the SF channel, after the temporal disturbance cancelation, we collect the samples from the available L polarimetric surveillance signals at the mth temporal observation in a $L \times 1$ vector $\mathbf{x}_n(m) = [x_n^{(0)}(m) \dots x_n^{(l)}(m) \dots x_n^{(L-1)}(m)]^T$, $m = 0, \dots, M - Q$, $n = 0, \dots, N - 1$. By assuming that that the corresponding process $\{\mathbf{x}_n(m)\}_{m=0}^{M-Q}$ follows a L–channel AR model of order $(Q - 1)$, a practical detector was derived based on a two-step GLRT approach followed by an additional adaptation stage [19]. The resulting detector is referred to as Mod-AR-Pol-AMF as it is given by

$$\mathbf{w}_n^H(\tau, f_D)\hat{\mathbf{D}}_n^{-1}(\tau, f_D)\mathbf{w}_n(\tau, f_D) \gtrless T_{Pol-AR} \tag{5}$$

where

$$\mathbf{w}_n(\tau, f_D) = \sum_{m=0}^{M-Q} \mathbf{\Upsilon}_n^H(m, \tau, f_D)\, \tilde{\mathbf{x}}_n(m) \tag{6}$$

Equation (6) shows that the obtained pol-time filter matrix $\mathbf{\Upsilon}_n(m, \tau, f_D)$ operates over consecutive and partially

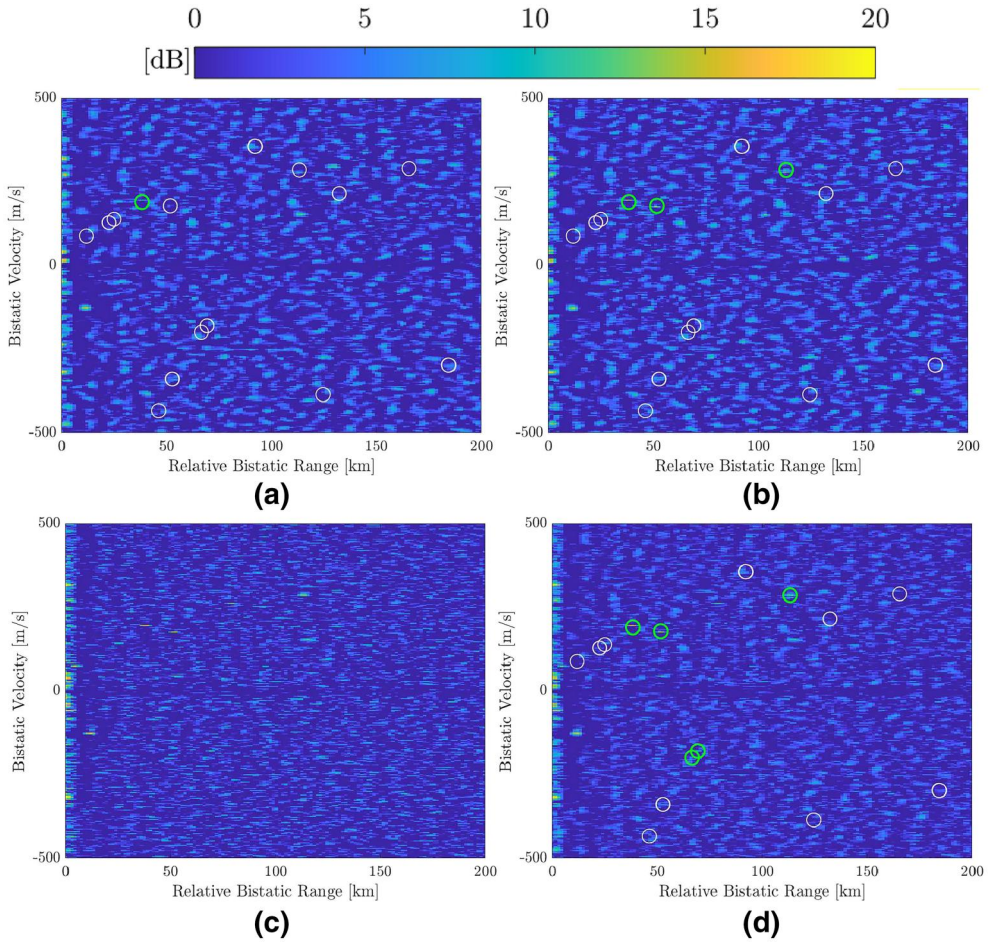

FIGURE 2 Range-velocity maps for a single datafile, evaluated at (a) H pol, (b) V pol, (c) H pol after polarimetric whitening, (d) output of the Pol-GLRT strategy

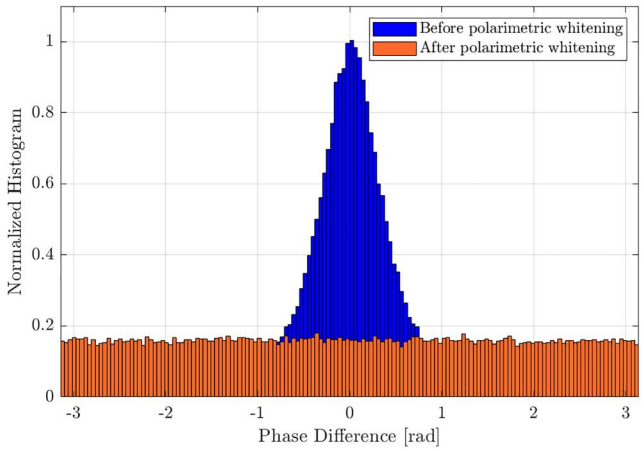

FIGURE 3 Histogram of phase difference measured at each range/Doppler location for a given datafile before and after polarimetric whitening

overlapped blocks of QL samples, defined as $\tilde{\mathbf{x}}_n(m) = \left[\mathbf{x}_n^H(m) \quad \mathbf{x}_n^H(m+1) \quad \ldots \mathbf{x}_n^H(m+Q-1)\right]^H$. Specifically, it is defined as

$$\Upsilon_n(m,\tau,f_D) = \hat{\mathbf{P}}_n^H(m)[\tilde{\mathbf{t}}_{n,0}(m,\tau) \otimes \mathbf{I}_L]e^{-j2\pi m\frac{f_D}{f_s}} \quad (7)$$

for a given CUT (τ, f_D), where f_s denotes the sampling frequency, $\mathbf{I}_L$ denotes the $L \times L$ identity matrix, and $\tilde{\mathbf{t}}_{n,0}(m,\tau)$ is defined in Table 2 as a Q–samples fragment of the transmitted waveform $r_n(t)$, delayed in time by τ being t_0 the CPI starting time. Furthermore, $\hat{\mathbf{P}}_n(m)$ is defined in Table 2 as the matrix of filter weights that operates a pol-time whitening of the data. Note that the estimation of the pol-time filter weights is repeated $\lceil (M-Q+1)/J \rceil$ times along the CPI and performed by averaging over blocks of J sub-CPIs each, resulting in a set of N_i matrices for each SF channels $\hat{\mathbf{P}}_{n,i}$, $i = 0, \ldots, N_i - 1$, $n = 0, \ldots, N-1$. Therefore, the filter weight matrix is updated as $\hat{\mathbf{P}}_n(m) = \hat{\mathbf{P}}_{n,\lfloor m/J \rfloor}$.

We recall that the selection of the parameter J is crucial for this detector to properly operate. In fact, it must be (i) large enough to guarantee a proper estimation of matrix $\hat{\mathbf{P}}_{n,i}$ and to assume that the target contribution is negligible with respect to the competing disturbance and (ii) short enough to adapt to the non-stationary characteristics of the disturbance. In this work we use $J = 200$ and we refer the interested reader to [21] for further details.

TABLE 2 Summary of the defined quantities

Quantity	Mathematical Expression	Definition
$\tilde{\mathbf{t}}_{n,0}(m,\tau)$	$\left[r_n\left(t_0+\frac{m}{f_s}-\tau\right) \quad \dots \quad r_n\left(t_0+\frac{m+Q-1}{f_s}-\tau\right)\right]^T$	$Q \times 1$ fragment of the transmitted waveform $r_n(t)$, delayed in time by τ being t_0 the CPI starting time
$\hat{\mathbf{P}}_{n,i}$	$\left[-\hat{\mathbf{A}}_{n,i}^H \mathbf{I}_L\right]^H \hat{\mathbf{R}}_{n,i}^{-1}\left[-\hat{\mathbf{A}}_{n,i}^H \mathbf{I}_L\right]$	$QL \times QL$ pol-time filter weights matrix at the ith block, $i = 0, \dots, N_i - 1$
$\hat{\mathbf{A}}_{n,i}$	$\hat{\mathbf{Q}}_{n,i,00}^{-1}\hat{\mathbf{Q}}_{n,i,01}$	$L \times L$ estimate complex-valued matrix parameters encoding the regression coefficients at different polarimetric channels
$\hat{\mathbf{R}}_{n,i}$	$\frac{1}{J}(\hat{\mathbf{Q}}_{n,i,11} - \hat{\mathbf{Q}}_{n,i,01}^H \hat{\mathbf{Q}}_{n,i,00}^{-1}\hat{\mathbf{Q}}_{n,i,01})$	$L \times L$ estimate of the polarimetric driving noise covariance matrix
$\hat{\mathbf{Q}}_{n,i}$	$\sum_{m=ij}^{(i+1)J-1}\tilde{\mathbf{x}}_n(m)\tilde{\mathbf{x}}_n{}^H(m) = \begin{bmatrix}\hat{\mathbf{Q}}_{n,i,00} & \hat{\mathbf{Q}}_{n,i,01}\\ \hat{\mathbf{Q}}_{n,i,01}^H & \hat{\mathbf{Q}}_{n,i,11}\end{bmatrix}$	$LQ \times LQ$ estimate of the pol-time disturbance covariance matrix within a sub-CPI of length Q. $\hat{\mathbf{Q}}_{n,i,00}$ $(L(Q-1)\times L(Q-1))$, $\hat{\mathbf{Q}}_{n,i,01}$ $(L(Q-1)\times L)$, $\hat{\mathbf{Q}}_{n,i,11}$ $(L \times L)$ are blocks of matrix $\hat{\mathbf{Q}}_{n,i}$

As demonstrated in [19], when the input disturbance does not strictly match with the employed AR model, vector $\mathbf{w}_n(\tau,f_D)$ is a L–dimensional complex Gaussian vector with a residual polarimetric covariance matrix $\mathbf{D}_n(\tau,f_D)$. Therefore, we estimate the latter using P i.i.d. and target-free secondary vectors, $\mathbf{w}_n(\tau_p,f_{Dp}), p \in I_{(\tau f_D)}$, $|I_{(\tau f_D)}| = P$, extracted from a set $I_{(\tau f_D)}$ of P indices that identify cells surrounding the CUT over the range-Doppler plane, as $\hat{\mathbf{D}}_n(\tau,f_D) = \sum_{p=1}^{P}\mathbf{w}_n(\tau_p,f_{Dp})\mathbf{w}_n^H(\tau_p,f_{Dp})$. Finally, under the assumption that the first adaptive cancellation stage meets the asymptotic condition, namely assuming that matrix $\hat{\mathbf{P}}_n(m)$ is built on asymptotic, though possibly mismatched, estimates of the AR parameters, the detection threshold $T_{Pol\text{-}AR}$ is found according to the P_{fa} expression in Equation (4), that only accounts for the fluctuations in the estimation of matrix $\hat{\mathbf{D}}_n$ due to finite P [19].

As for the Pol-GLRT, we first investigate the effectiveness of this approach in Figure 4, where we report the results obtained over the same single datafile shown in Figure 2. Specifically, the output of the Mod-Pol-AR-AMF strategy, right before the thresholding stage, scaled to the noise floor power level. By comparing Figure 2 and 4 (i) the improvement with respect to the maps at the SP channels (Figure 2a,b) is evident as the background disturbance level is substantially reduced; (ii) the result obtained with the Mod-Pol-AR-AMF is slightly better than to the one of the Pol-GLRT (Figure 2d) at this datafile, revealing that the disturbance has been more effectively rejected and additional detections are obtained.

In order to completely assess the performance of the polarimetric detectors, Section 3.3 will be devoted to carry out an extensive analysis.

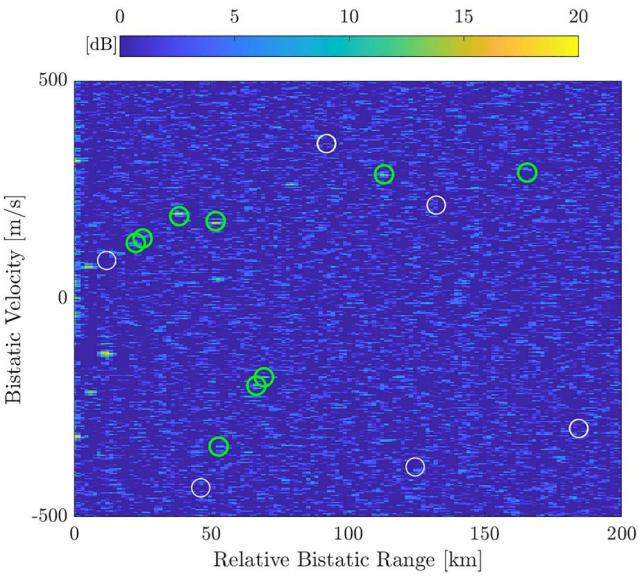

FIGURE 4 Range-velocity maps for the datafile used in Figure 5, evaluated at after Mod-Pol-AR-AMF with $Q = 3$

3.3 | Extensive experimental validation

To investigate the target detection capability against a grid of false alarm rate values, we evaluated the empirical receiver operating characteristic (ROC) curves. At each data file, and for a given considered false alarm rate value, a correct detection is declared when a peak in the range-Doppler plane exceeded the selected threshold at the radar coordinates predicted by the available air-truth plus a small tolerance. Then, the detection frequency is obtained by dividing the number of correct detections by the maximum number of target occurrences across the entire dataset, namely 9632. Note that the detection analysis is limited to targets laying in the range-band (0–100) km and included within an angular sector of 90° around the surveillance antenna pointing direction.

In Figure 5 we show the obtained empirical ROC curves using the mentioned polarimetric adaptive strategies for the FM radio channel f_2. Note that the Mod-Pol-AR-AMF is applied with $Q = 3$ while $P = 32$ is assumed for all considered strategies. The results obtained with the Pol-NCI and when the polarization diversity is not exploited, and the conventional single-channel PCL processing is separately applied to the V and H polarization, are also shown for comparison.

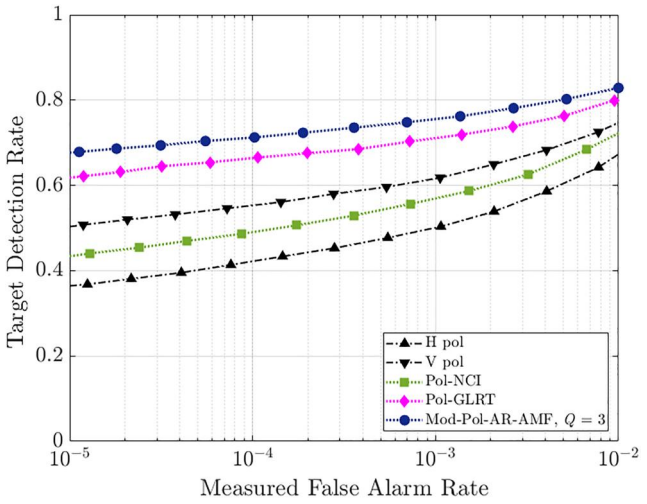

FIGURE 5 Empirical ROC curves at f_2

From Figure 5, the following considerations apply:

- The target detection rate separately obtained at the two SP channels is significantly different. Moreover, it was shown in [16] that the detection performance of a given SP channel varies with the employed frequency channel.
- The Pol-NCI is not able to effectively exploit the polarimetric information to improve the target detection performance and it might even yield a worse target discrimination capability with respect to a SP channel. This is due to the generally higher number of false alarms obtained, which confirms the weakness of the assumption of independent disturbance at the different polarimetric channels, thus the unsuitability of this solution.
- Both strategies that adaptively exploits the polarimetric correlation characteristics to counteract the disturbance, namely the Pol-GLRT and the Mod-Pol-AR-AMF, yield a substantial improvement with respect to both the SP solutions and the Pol-NCI. However, thanks to a suitable exploitation of both the polarimetric and temporal correlation, the Mod-Pol-AR-AMF enhances the target detection capability of approx. 7%-8% with respect to the Pol-GLRT. Moreover, the detector described in Section 3.2 yields a tremendous improvement of approx. 30% and 67%, measured at $P_{fa} = 10^{-4}$, with respect to the conventional PCL processing applied to the V pol and H pol channels, respectively.

Based on these considerations, and given the substantial advantage offered by the Mod-Pol-AR-AMF, the purpose of the next sections is to extend this approach to a MF scenario, aiming at further improving the target detection performance of the PCL sensor.

In order to understand the content of the next sections with sufficient knowledge of past approaches using frequency diversity and polarization separately, Sections 2 and 3 briefly covered these topics. Table 3 summarizes all the strategies mentioned, supported by the appropriate references, that we invite the interested reader to refer to for further details.

TABLE 3 Summary of multi-frequency and multi-polarimetric detectors

Detector	Operative Domain	References
Centralized MF-NCI	Frequency	[11, 12]
Pol-NCI	Polarization	[13, 16]
Pol-GLRT	Polarization	[16, 17]
Mod-ol-AR-AMF	Polarization-time	[18–21]

4 | MULTI-FREQUENCY AND MULTI-POLARIMETRIC AR MODEL BASED ADAPTIVE MATCHED FILTER

In this section, we build upon the demonstrated benefits shown in Section 3 and we derive a new adaptive target detector that jointly exploits the information diversity offered by signals simultaneously collected via multi-polarized antennas at multiple carrier frequencies.

To this purpose, we consider the NL signals available after they separately underwent the first temporal disturbance cancelation stage. Then, to benefit from the disturbance rejection at the SF channel based on the polarimetric and temporal information, we filter the data via matrix $\boldsymbol{\Upsilon}_n(m,\tau,f_D)$, to obtain the NL–dimensional complex vectors $\mathbf{w}_n(\tau,f_D) = \sum_{m=0}^{M-Q} \boldsymbol{\Upsilon}_n^H(m,\tau,f_D)\,\tilde{\mathbf{x}}_n(m)$, $n = 0, \ldots, N-1$ for a given CUT (τ,f_D). Note that the filter weights contained in $\boldsymbol{\Upsilon}_n(m,\tau,f_D)$ are separately updated at each SF channel, assuming the disturbance independent at different carrier frequencies.

Under the asymptotic conditions, each vector $\mathbf{w}_n(\tau,f_D)$ after the pol-time filtering, is assumed to be complex Gaussian distributed, with covariance matrix $\hat{\mathbf{D}}_n(\tau,f_D)$, zero-mean vector under the H_0 hypothesis ($\gamma = 0$) and mean vector $\mathbf{s}_n$ under the H_1 hypothesis ($\gamma = 0$), that is $\mathbf{w}_n(\tau,f_D) \sim \mathcal{CN}(\gamma\mathbf{s}_n, \hat{\mathbf{D}}_n(\tau,f_D))$. In detail, vector $\mathbf{s}_n = [\alpha_{n,0} \ \ldots \ \alpha_{n,l} \ \ldots \ \alpha_{n,L-1}]^T$, where $\alpha_{n,l}$, $l = 0, \ldots, L-1$, $n = 0, \ldots, N-1$, is the target unknown complex amplitude at the lth polarimetric channel and nth frequency channel. To simplify the notation, in the following we use $\mathbf{w}_{n,0} = \mathbf{w}_n(\tau,f_D)$ and $\mathbf{D}_{n,0} = \mathbf{D}_n(\tau,f_D)$. Finally, a set of P target-free secondary vectors is assumed available at each frequency channel, say $\mathbf{w}_{n,p} = \mathbf{w}_n(\tau_p,f_{Dp})$, $n = 0, \ldots, N-1$, $p = 1, \ldots, P$, $p \in I_{(\tau,f_D)}$, $|I_{(\tau,f_D)}| = P$. They are extracted from a set $I_{(\tau,f_D)}$ of P indices that identify cells surrounding the CUT over the range-Doppler plane and they are assumed to share the same statistics as the CUT under the null hypothesis, that is $\mathbf{w}_{n,p} \sim \mathcal{CN}(\mathbf{0}_{L\times 1}, \mathbf{D}_{n,0})$. Under these hypotheses, we derive the

sought detector by resorting to the same method used in [22], as:

$$L\left(\begin{array}{c}\{\mathbf{w}_{p,n}\}\ n=0,\ \ldots,\ N-1\\ p=0,\ \ldots,\ P\end{array}\right) = \prod_{n=0}^{N-1} L^{(n)}\left(\{\mathbf{w}_{p,n}\}_{p=0,\ \ldots,\ P}\right) \gtrless T \tag{8}$$

where T is the detection threshold, $L(\cdot)$ represents the likelihood ratio and the likelihood ratio at the nth carrier frequency is given by

$$L^{(n)}\left(\{\mathbf{w}_{p,n}\}_{p=0,\ \ldots,\ P}\right) = \frac{\max\limits_{\mathbf{s}_n,\mathbf{D}_{n,0}}\left\{p_{\mathbf{w}_n}(\mathbf{w}_{n,0}\mid H_1)\prod_{p=1}^{P}p_{\mathbf{w}_n}(\mathbf{w}_{n,p}\mid H_0)\right\}}{\max\limits_{\mathbf{D}_{n,0}}\left\{p_{\mathbf{w}_n}(\mathbf{w}_{n,0}\mid H_0)\prod_{p=1}^{P}p_{\mathbf{w}_n}(\mathbf{w}_{n,p}\mid H_0)\right\}} \tag{9}$$

$$n=0,\ \ldots,\ N-1$$

By proceeding as in [22] for each factor independently, we finally obtain

$$\prod_{n=0}^{N-1}\left[\mathbf{w}_{n,0}^{H}\hat{\mathbf{D}}_{n,0}^{-1}\mathbf{w}_{n,0}+1\right] \gtrless T_{MF\&MP-AR-AMF} \tag{10}$$

where $T_{MF\&MP-AR-AMF}$ is the detection threshold and $\hat{\mathbf{D}}_{n,0}^{-1}=\sum_{p=1}^{P}\mathbf{w}_{n,p}\mathbf{w}_{n,p}^{H}$. A closed form expression for the P_{fa} is reported in [22] and can be used to select the appropriate detection threshold for a given desired P_{fa}.

The derived target detector in Equation (10) will be referred to in the following as multi-frequency and multi-polarimetric AR model based adaptive matched filter (MF&MP-AR-AMF) and a block diagram of the entire processing scheme is sketched in Figure 6. Note that, for $N=1$, the proposed solution corresponds to the Mod-Pol-AR-AMF in Equation (5) with $T_{Pol-AR} = T_{MF\&MP-AR-AMF}-1$.

The performance of the MF&MP-AR-AMF will be investigated in the following section in comparison with the strategies described in Sections 2 and 3 as well as with the MF&MP solution proposed in [22] and referred to as MF&MP-GLRT. In detail, the latter was obtained as an extension of the Pol-GLRT described in Section 3.1 to a MF scenario. The MF&MP-GLRT detector is given by

$$\prod_{n=0}^{N-1}\left[\mathbf{y}_n^{MP\,H}\hat{\mathbf{M}}_{n,0}^{-1}\mathbf{y}_n^{MP}+1\right] \gtrless T_{MF\&MP-GLRT} \tag{11}$$

where $\mathbf{y}_n^{MP}$ is $L\times 1$ complex vector that collects the outputs at a given CUT of the L CAFs separately obtained at the different polarimetric channels and for the nth frequency channel, with no prior rejection of the disturbance.

5 | PERFORMANCE ASSESSMENT AND COMPUTATIONAL COMPLEXITY

In this section, we carry out an extensive experimental validation of the proposed MF&MP-AR-AMF detection strategy aimed at assessing its benefits in comparison with alternative target detectors.

First, in Section 5.1 we investigate the achievable performance with the proposed target detection strategy compared to the one offered by the alternative MF&MP solution presented in [22]. Then, in Section 5.2, we compare the obtained results with the strategies recalled in Sections 2 and 3 that separately leverage the polarimetric and frequency information.

5.1 | Comparison with state-of-the-art MF&MP detector

First, we investigate the performance obtained with the Mod-Pol-AR-AMF, or equivalently of the MF&MP-AR-AMF with $N=1$, at the different available frequency channels and with different number Q of taps. To this end, we report in Figure 7 the target detection rate measured at $P_{fa}=10^{-4}$ for the four available FM radio channels.

From Figure 7, some interesting considerations can be deducted. First, we notice a considerable difference in terms of target detection capability between the different frequency channels, that suggests the joint combination of the signals collected at different carrier frequencies as a way to further improve the final performance. However, though the achievable performance changes with the employed SF channel, all of them exhibit a similar behaviour. Specifically, the target detection rate always improves from $Q=1$, namely when the employed filter only exploits the polarimetric diversity, to $Q\geq 2$, confirming that the temporal correlation of the disturbance should be considered. Then, depending on the employed frequency channel, different Q values yield slightly different results and, as the AR model order further grows, the improvement starts decreasing due to non-negligible loss. However, the analysis suggests that a Q value included in the interval between $Q=3$ and $Q=7$ would be a reasonable choice for all exploited FM radio channels. However, as pointed out in [21], the choice of the employed parameters is also driven by further considerations, including the overall complexity, which will also tend to grow when $N>1$. Therefore, based on the reported results, a number $Q=3$ of taps will be used in the following.

Once the performance of the MF&MP-AR-AMF has been assessed in a SF scenario, it is interesting to investigate its advantage with respect to the state-of-the-art solution, namely the MF&MP-GLRT.

We first study the capability of the two MF&MP adaptive detectors to control the false alarm rate. To this purpose, we

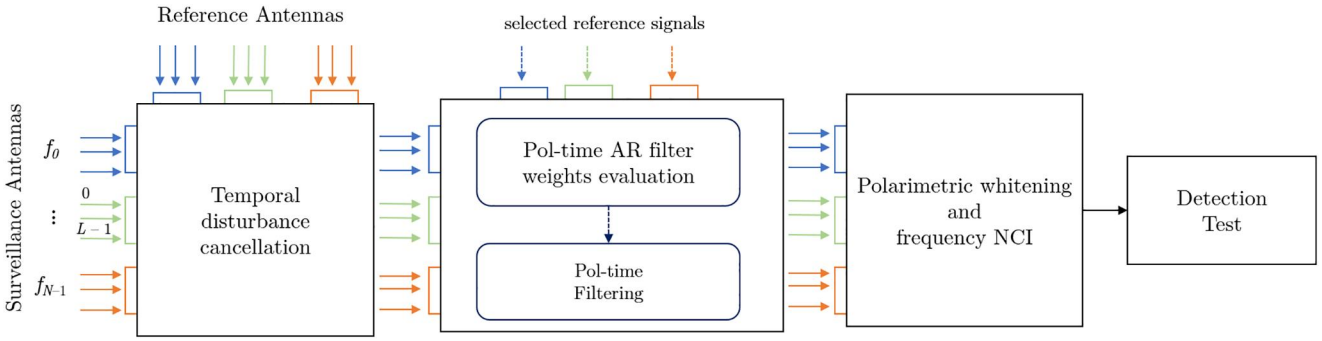

FIGURE 6 Processing scheme of the MF&MP–AR–AMF

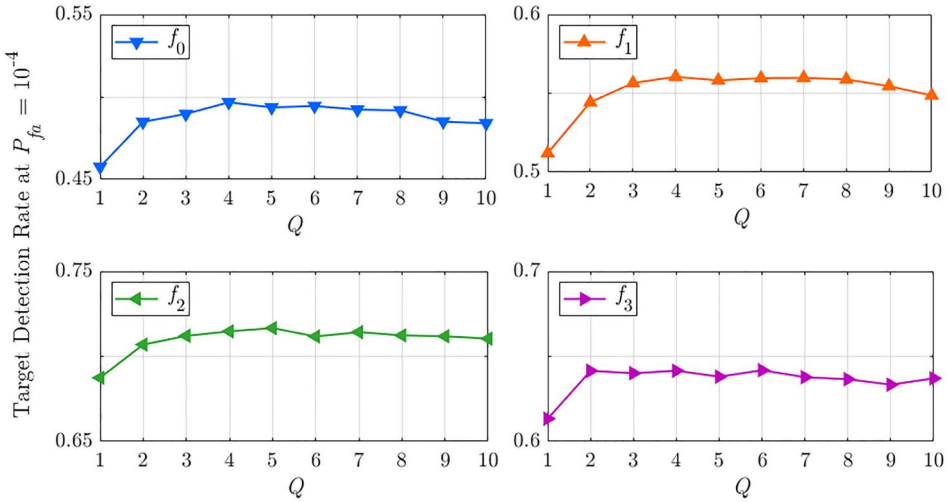

FIGURE 7 Target detection rate obtained with the Mod-Pol-AR-AMF at $P_{\text{fa}} = 10^{-4}$ versus Q for different FM radio channels

report in Figure 8 the false alarm rate versus the nominal value for different N. Note that we measure the false alarm rate in the range band [150–200] km where the detection probability is very low so that it is unlikely to include and label as false alarms detections corresponding to targets not equipped with a transponder and therefore not identified by the available air-truth. In all subfigures, magenta lines represent the results obtained with the MF&MP-GLRT while blue lines represent the results of the MF&MP-AR-AMF. Incidentally, we note that two different selections of frequency channels are used when $N = 2$, namely $\{f_0, f_1\}$ and $\{f_2, f_3\}$. They correspond to the worst and best performing pair of frequency channels, respectively. From Figure 8, we can conclude that both multi-channel adaptive target detection strategies yield an acceptable capability of controlling the false alarm rate, with the measured P_{fa} being only slightly higher than the desired one.

This result also demonstrates that the assumption of asymptotic estimation of the AR pol-time filter weights [21], separately performed at each frequency channel in the MF&MP-AR-AMF solution, stands. On the contrary, the slight deviation from the desired value might be mostly related to the availability of P training data for the residual polarimetric covariance matrix estimation.

Then, we study the target detection performance in Figure 9. Specifically, we report the target detection rate obtained at a measured $P_{fa} = 10^{-4}$ for the same selections of frequency channels made in Figure 8. Also in this case, magenta markers denote the MF&MP-GLRT solution while blue markers correspond to the proposed MF&MP-AR-AMF approach.

From Figure 9, the following comments are in order:

i. When the same number of receiving channels is employed, the target detection capability of the MF&MP-AR-AMF is always higher than the MF&MP-GLRT.
ii. When $N = 1$, namely when the frequency diversity is not exploited, the improvement offered by the MF&MP-AR-AMF varies from one frequency channel to another. As an example, when f_1 is used, the obtained improvement is approx. 20% on average which corresponds to more than 880 additional detections. The improvement is more apparent at frequency channels yielding worse performance as those are the most likely affected by severe interference.
iii. The higher is the number N of frequency channels that are jointly combined, the smaller is the measured improvement. This is because combining signals received at

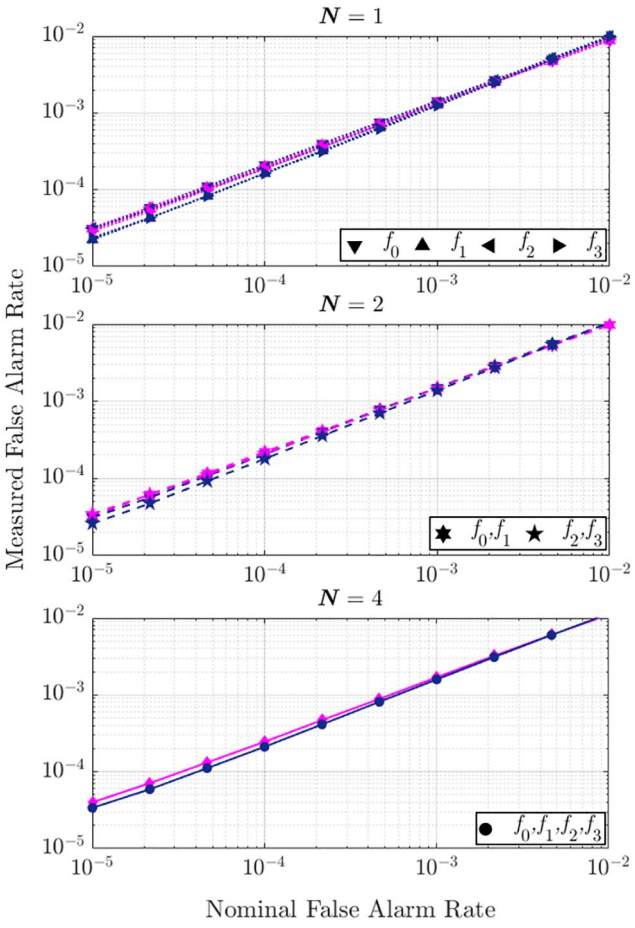

FIGURE 8 Measured versus Nominal false alarm rate for MF&MP-AR-AMF (blue lines) and MF&MP-GLRT (magenta lines) for different N

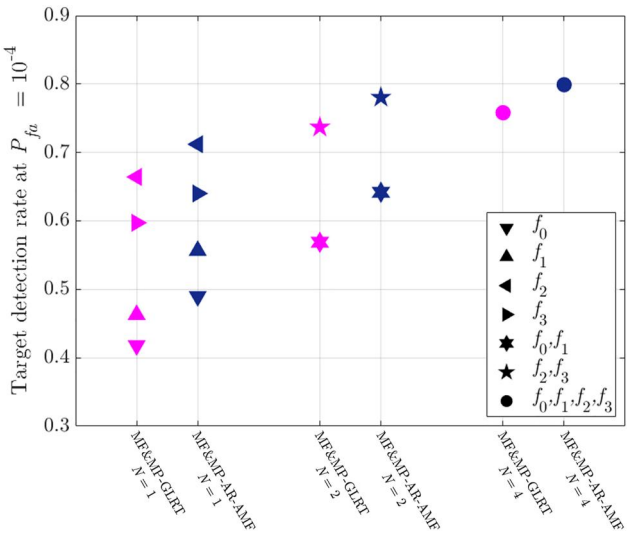

FIGURE 9 Target detection rate obtained at a measured $P_{\text{fa}} = 10^{-4}$ for MF&MP-AR-AMF (blue markers) and MF&MP-GLRT (magenta markers) for different N

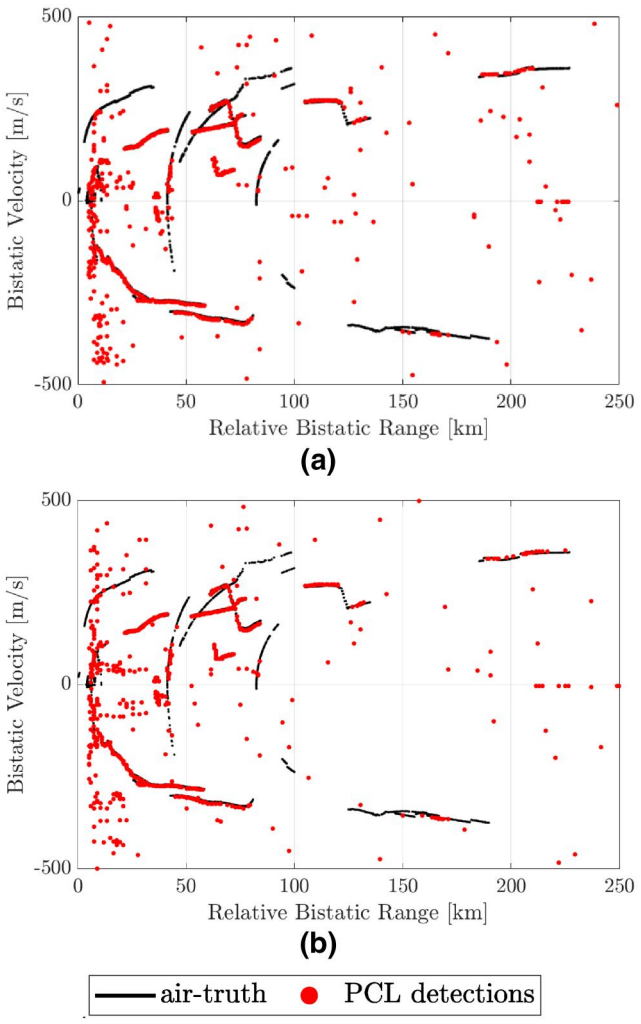

FIGURE 10 Detection results over 50 consecutive datafiles, with $P_{\text{fa}} = 10^{-5}$, using: (a) MF&MP-GLRT, $N = 4$ (f_0, f_1, f_2, f_3); (b) MF&MP-AR-AMF, $N = 2$ (f_2, f_3)

multiple carrier frequencies generally mitigates the disturbance affecting the SF channel.

iv. When $N = 2$ the difference between the best and worst performing pair of frequency channels in terms of target detection capability is substantial.

v. It is noteworthy that when (f_2, f_3) are jointly used, the target detection rate obtained with the proposed MF&MP-AR-AMF strategy is higher than the one obtained using the state-of-the-art MF&MP-GLRT detector that jointly combines all available FM radio channels ($N = 4$). This confirms that the performance enhancement operated at the SF channel is a key stage in the entire processing scheme and paves the way for considerations about the possibility of reducing the number receiving channels, if properly exploited.

To see what the last consideration practically means we report in Figure 10, the raw detections obtained for 50 consecutive datafiles for $P_{fa} = 10^{-5}$ over the same bistatic range-velocity plane. The available air-truth is shown in black

TABLE 4 Computational complexity

	FLOPs
MF&MP-GLRT	$O\{NL\ N\tau\ [8M\ log_2(M) + 6M] + NN\tau\ N_f\ PL\ (4L + 5)\}$
MF&MP-AR-AMF	$O\{NL\ N\tau\ 8\ [(M - Q + 1)\ log_2(M - Q + 1) + LQJ + 4N\ (M - Q + 1)\ (LQ)^2 + NN\tau\ N_f\ PL\ (4L + 5)\}$

while the PCL detections are denoted by red dots. Figure 10a shows the results of the MF&MP-GLRT performed with $N = 4$ (f_0, f_1, f_2, f_3) while Figure 10b shows the results obtained when using the proposed MF&MP-AR-AMF approach with $N = 2$ (f_2, f_3).

Figure 10 clearly confirms the last consideration made on Figure 9, showing that the two solutions yield comparable results though the MF&MP-AR-AMF is using half of the frequency channels exploited by the MF&MP-GLRT.

As mentioned, this result suggests the possibility of not using all available frequency channels. Obviously, this would require a prior analysis aimed at understanding which FM radio channels are best performing, however, this is a procedure that is generally already in place when selecting the carrier frequencies to be collected. The main advantage is expected to be a significant reduction in terms of computational load.

To further investigate the latter point, we study the computational complexity of the two MF&MP target detectors in Table 4. Specifically, we report the order of magnitude of the number of needed floating-point operations (FLOPs), expressed as a function of the relevant parameters.

We assume that a complex addition requires two FLOPs and a complex multiplication requires six FLOPs. The total number of delay and Doppler bins are denoted in Table 4 as $N\tau$ and N_f, respectively. By observing Table 4, the different components of the computational burden are clearly identified. In detail, for the MF&MP-GLRT approach, the component that requires the highest computational complexity is the evaluation of LN range-velocity maps. We assume to carry that out using an efficient algorithm described in [2] and referred to as Direct–FFT which requires $N\tau[8M\ \log_2(M) + 6M]$ FLOPs for each CAF.

On the other hand, the processing stages foreseen in the MF&MP-AR-AMF strategy that require the highest number of FLOPs are the pol-time AR filter construction and application, to be repeated N times. For additional details on the computational complexity required by the MF&MP-AR-AMF for the $N = 1$ case, see [21].

Finally, the cost required for the polarimetric whitening in the range-Doppler plane, the frequency integration and the detection test is equal in both cases and it is mainly constituted by the estimation and inversion of the $L \times L$ covariance matrix, based on P training data, to be repeated $N\tau\ N_f$ times for each FM radio channel. As expected, the additional processing stages foreseen in the MF&MP-AR-AMF approach increase the computational complexity with respect to the alternative MF&MP strategy.

However, in order to further explore this aspect and quantitatively evaluate this result, a detailed numerical analysis is required in a practical scenario. To this end, we refer to the case of a multi-channel PCL system exploiting N signals in the FM radio band for aerial surveillance, and we report in Figure 11 the total number of required FLOPs versus the employed CPI. We assume a maximum relative bistatic range of 200 km and a maximum bistatic velocity of 500 m/s. The sampling frequency is assumed as $f_S = 200$ kHz and, while $P = 32$, and $Q = 3$. We compare the number of FLOPs required by the 2 MF&MP detectors for different values of N and we report the case of MF-NCI and SF&SP solutions for comparison.

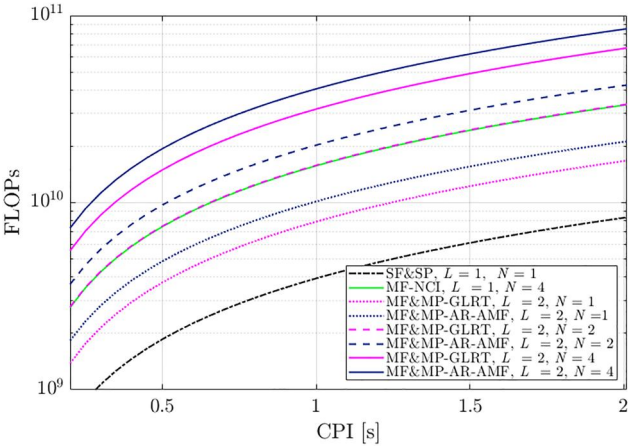

FIGURE 11 Computational complexity versus CPI for different solutions

Figure 11 confirms that the computational complexity of MF&MP-AR-AMF is slightly higher than the MF&MP-GLRT, and the comparison between the two adaptive detectors does not change as the number N of integrated FM radio channels varies.

However, the increase in terms of the number of FLOPs is below 20% for the selected parameters. By recalling that, with reference to the considered dataset, the proposed detector potentially allows to halve the number N of frequency channels compared to its counterpart while still maintaining better performance, the final complexity might be even lower. It is worth stressing the point that the obtained result highly depends on the quality of the available FM radio channel, however, we recall that also when exploiting the same channels, the MF&MP-AR-AMF shows superior performance with respect to the MF&MP-GLRT while requiring only a slightly higher complexity. Once the increased effectiveness of the proposed approach has been demonstrated compared to the alternative strategy that jointly exploits polarimetric and frequency diversity and the computational burden has been studied, we

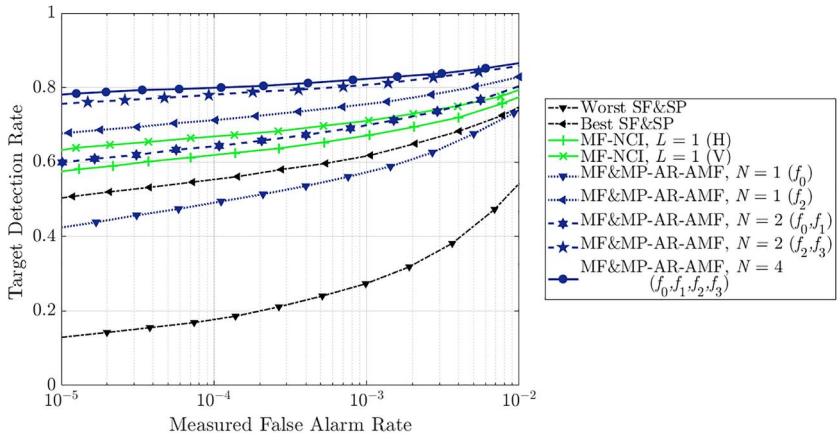

FIGURE 12 Empirical ROC curves for different detectors

complete the performance analysis by also considering alternative detectors, which is the purpose of Section 5.2.

5.2 | Comparison with MF&SP and SF&MP detectors

Figure 12 shows the empirical ROC curves obtained with different approaches as listed below:

- a conventional PCL processing scheme applied to the best and worst pair of SF&SP channels (black lines),
- the MF&NCI approach described in Section 2 operated with $N = 4$ at the H and V polarimetric channels (green lines),
- the MF&MP-AR-AMF with $L = 2$ and $N = 1$, 2 and 4 (dark blue lines). Incidentally, we recall that the case of MF&MP-AR-AMF with $N = 1$ corresponds to the polarimetric adaptive detector described in Section 3.2.

Based on Figure 12, the following final comments apply:

- The target detection performance obtained at a single channel can dramatically change depending on the employed polarization and FM radio channel. From Figure 11 it is evident that this solution is the least expensive from a computational point of view, however its performance does not justify the obtained computational burden reduction.
- The frequency integration operated at the SP channel (MF-NCI approach with $N = 4$) remarkably improves the achievable performance and increases the robustness of the system by averaging good and bad FM radio channels.
- When the signals collected with multi-polarized antennas at a SF channel are properly combined according to the proposed approach, the improvement with respect to the SF&SP solutions is terrific. Moreover, if the SF channel is properly selected (f_2), the proposed detector can even outperform the MF-NCI solution, though using half of the receiving channels ($L = 2$ vs. $N = 4$), thus requiring a lower computational load of approx. 35%.
- When using the MF&MP-AR-AMF with $N = 2$ and the best pair of frequency channels is selected (f_2, f_3), the obtained target detection capability is substantially higher with respect to the MF-NCI detector. For instance, an improvement of 15% and 25% is obtained at $P_{\text{fa}} = 10^{-4}$ with respect to the MF-NCI at the best (V) and worst (H) SP channel, respectively. This result is obtained with only a slightly higher computational complexity with respect to the MF-NCI solution with $N = 4$ (see dashed blue and solid green curves in Figure 11). Moreover, it is worth recalling that the performance achievable with the MF-NCI approach highly depend on the quality of the available frequency channels.
- Finally, as also shown in Figure 9, MF&MP-AR-AMF approach exploiting all available degrees of freedom ($L = 2$ and $N = 4$) is the best performing solution, properly counteracting the competing disturbance and further improving the system robustness with respect to the time-varying characteristics of the employed waveform and propagation channel.

In order to get a practical idea of how the different strategies compare, we report in Figure 13 the raw detections obtained for the same 50 consecutive scans used in Figure 13 with $P_{fa} = 10^{-5}$. In detail, we compare the results of the MF approach described in Section 2 applied at the best SP channel (V) in Figure 13a, the results of the MP approach described in Section 3.2 applied at the best SF channel (f_2) in Figure 13b and the derived MF&MP-AR-AMF strategy with $L = 2$ and $N = 4$ in Figure 13c. The results in Figure 13 clearly confirm the considerations above. In fact, comparing the MF&SP (Figure 13a) and SF&MP (Figure 13b) approaches, the two strategies yield comparable detection although the SF&MP is using less receiving channels. For instance, Figure 13a has a higher number of detection in the track at [210–230] km, while Figure 13b shows additional plots for the target rapidly crossing the zero-Doppler at 40 km, both highlighted by the green arrow in the respective figure. Finally, the combination of both polarimetric and frequency diversity according to the proposed detector (Figure 13c) yields additional detections at almost every track, even at further ranges. See for instance the target track at

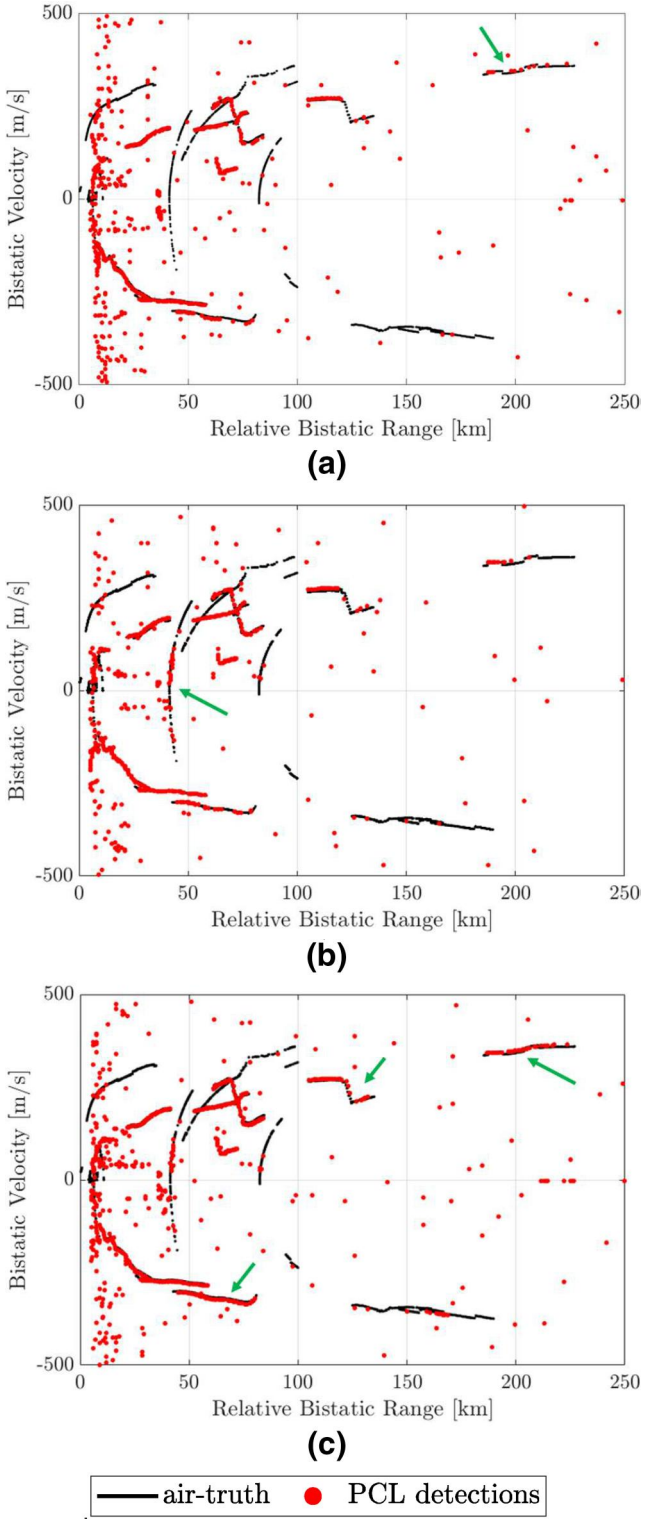

FIGURE 13 Detection results over 50 consecutive datafiles, with $P_{fa} = 10^{-5}$, using: (a) MF-NCI, $L = 1$ (V), $N = 4$ (f_0, f_1, f_2, f_3); (b) MF&MP-AR-AMF, $L = 2, N = 1$ (f_2); (c) MF&MP-AR-AMF, $L = 2, N = 4$ (f_0, f_1, f_2, f_3)

[50–100] km and approx. −330 m/s and the one at [210–230] km and approx. 350 m/s, that are now detected with very good continuity (see green arrows). In conclusion, the MF&MP-AR-AMF is confirmed to be the best performing strategy not only with respect to the approaches in Figure 13a,b but also with respect to the MF&MP-GLRT using the same receiving channels (Figure 10a).

The experimental results shown in this section demonstrate the effectiveness of the proposed solution against FM radio transmissions. Similar advantages are expected when using different broadcast signals as waveforms of opportunity.

6 | CONCLUSION

A new multi-channel model based adaptive target detector for passive radar systems is derived in this work. The proposed detection strategy effectively leverages the information diversity obtained collecting, with multi-polarized antennas, signals simultaneously transmitted by the same illuminator of opportunity at different carrier frequencies. The extensive experimental validation carried out against FM radio-based PCL data clearly demonstrates the improvement offered by the conceived solution in terms of target detection capability. The obtained benefits are due to both a proper disturbance rejection at the SF channel, thanks to a fruitful exploitation of the polarimetric and temporal correlation and to the integration of the target echo at the different frequency channels. Moreover, we show that an effective reduction of the interference sources at the SF channel potentially allows reducing the number of necessary frequency channels to achieve good results, thus reducing the overall required computational burden.

ORCID

Francesca Filippini https://orcid.org/0000-0001-7821-0065
Fabiola Colone https://orcid.org/0000-0002-6694-7534

REFERENCES

1. Griffiths, H.D., Baker, C.J.: Passive coherent location radar systems. Part 1: performance prediction. IEE Proc. Radar, Sonar Navig. 152(3), 153–159 (Jun. 2005)
2. Lombardo, P., Colone, F.: Advanced processing methods for passive bistatic radar systems. In: Melvin, W.H., Scheer, J.A. (eds.) Principles of Modern Radar: Advanced Techniques, pp. 739–821. Schitech Publisher (2012)
3. Howland, P.E., Maksimiuk, D., Reitsma, G.: FM radio based bistatic radar. IEEE Proc. Radar, Sonar Navig, vol. 152, pp. 107–115 (3 Jun. 2005)
4. Saini, R., Cherniakov, M.: DTV signal ambiguity function analysis for radar application. IEEE Proc. Radar, Sonar Navig. 152(3), 133–142 (Jun. 2005)
5. Palmer, J.E., et al.: DVB-T passive radar signal processing. IEEE Trans. Signal Process. 61(8), 2116–2126 (2013)
6. Coleman, C., Yardley, H.: Passive bistatic radar based on target illuminations by digital audio broadcasting. IET RSN. 2(5), 366–375 (Oct. 2008)
7. Poullin, D.: Passive detection using digital broadcasters (DAB, DVB) with COFDM modulation. IEE Proc. Radar, Sonar Navig. 152(3), 143–152 (Jun. 2005)
8. Olsen, K.E., Woodbridge, K.: Performance of a multiband passive bistatic radar processing scheme – part I. IEEE Aerosp. Electron. Syst. Mag. 27(10), 16–25 (Oct. 2012)
9. Woodbridge, K., Olsen, K.E.: Performance of a multiband passive bistatic radar processing scheme – part II. IEEE AES Mag. 27(11), 4–14 (Nov. 2012)

10. Zaimbashi, A.: Multiband FM-based passive bistatic radar: target range resolution improvement, in IET Radar, Sonar Navig., vol. 10, no. 1, pp. 174-185, 1 (2016)
11. Colone, F., Bongioanni, C., Lombardo, P.: Multifrequency integration in FM radio-based passive bistatic radar. Part I: target detection. IEEE Aerosp. Electron. Syst. Mag. 28(4), 28–39 (2013)
12. Martelli, T., et al.: Multi-frequency target detection techniques for DVB-T based passive radar sensors. Sensors. 16, 1594 (2016)
13. Bongioanni, C., et al.: Exploiting polarimetric diversity to mitigate the effect of interferences in FM-based passive radar. In: 11-th International Radar Symposium, Vilnius, pp. 1–4 (2010)
14. Conti, M., Moscardini, C., Capria, A.: Dual-polarization DVB-T passive radar: experimental results. IEEE Radar Conference, Philadelphia, PA pp. 1–5 (2016)
15. Cabrera, O., et al.: Detecting drones and human beings with DVB-S based COTS passive radar for short-range surveillance. In: 2020 IEEE International Radar Conference (RADAR) Washington, DC, USA, pp. 37–42 (2020)
16. Colone, F., Lombardo, P.: Polarimetric passive coherent location. IEEE Trans. Aerosp. Electron. Syst. 51(2), 1079–1097 (2015)
17. Filippini, F., et al.: Experimental results of polarimetric detection schemes for DVB-T-based passive radar. IET Radar, Sonar Navig. 11(6), 883–891 (6 2017)
18. Colone, F., Filippini, F.: Auto-regressive model based polarimetric adaptive detection scheme. Part I: theoretical derivation and performance analysis. IEEE Trans. Aerosp. Electron. Syst. 56(5), 3762–3778 (2020)
19. Colone, F., Filippini, F.: Auto-regressive model based polarimetric adaptive detection scheme. Part II: performance assessment under spectral model mismatch. IEEE Trans. Aerosp. Electron. Syst. 56(5), 3779–3795 (2020)
20. Filippini, F., Colone, F.: Polarimetric detection scheme for passive radar based on a 2D auto-regressive disturbance model. In: 2019 International Radar Conference (RADAR) Toulon, France, pp. 1–6.(2019)
21. Filippini, F., Colone, F.: Polarimetric passive radar: a practical approach to parametric adaptive detection. IEEE Trans. Aerosp. Electron. Syst. 56(6), 4930–4946 (2020)
22. Colone, F., Lombardo, P.: Non-coherent adaptive detection in passive radar exploiting polarimetric and frequency diversity. IET RSN. 10(1), 15–23 (1 2016)
23. Filippini, F., Colone, F.: Multi-carrier adaptive detection in polarimetric passive radars. In: Proc. 2020 IEEE Radar Conference, Florence (2020)
24. Colone, F., et al.: Sliding extensive cancellation algorithm for disturbance removal in passive radar. IEEE Trans. Aerosp. Electron. Syst. 52(3), 1309–1326 (2016)

How to cite this article: Filippini F, Colone F. Multi-carrier and multi-polarimetric model based adaptive target detector for passive radar systems. *IET Radar Sonar Navig*. 2021;1−14. https://doi.org/10.1049/rsn2.12061